Individual Tree Crown Detection and Delineation From Very-High-Resolution UAV Images Based on Bias Field and Marker-Controlled Watershed Segmentation Algorithms

Hongyu Huang , Xu Li, and Chongcheng Chen

Abstract—**Individual tree crown detection and delineation (ITCD) mainly depend on high-resolution aerial photos and satellite images or LiDAR, and these data can be costly to obtain. The advent of unmanned aerial vehicle (UAV) remote sensing technology provides an economic and effective method for data acquisition. Therefore, the research of ITCD based on UAV high-resolution images is of significance to improve the efficiency and accuracy of forest resource inventory and remote sensing validation. However, in very high-resolution (defined here with the pixel size smaller than 10 cm) images, the inhomogeneities in the canopy texture can be detrimental to the correct detection of individual trees by computer processing. We applied the bias field estimation, which is used in medical image segmentation, to reduce the within-canopy spectral heterogeneity in the very high-resolution UAV-derived orthophoto. By selecting young *Osmanthus* and *Podocarpus* trees that grow in a nursery as the study objects, we tested our method in an orthophoto (with a ground resolution of 2.5 cm) generated from overlapping UAV images. A local intensity clustering was first applied to produce a smoothed bias field image; then, by using morphological operation of opening and closing, the fine texture of the canopy was further smoothed. Finally, individual tree crowns were extracted by applying the marker-controlled watershed segmentation algorithm. The segmentation results were validated by comparing to the manually drawn individual tree crown polygons. The *F*-scores of the detection rate for *Osmanthus* and *Podocarpus* were 98.2% and 93.1%, respectively. The result is considerably better than those achieved with similar processing steps but without the bias field treatment. Our study proves that it is feasible and effective to detect and delineate individual tree crowns based on the bias field and marker-controlled watershed segmentation in very-high-resolution images obtained from UAV.**

Index Terms—**Bias field, canopy detection, drone remote sensing, forest inventory, single tree extraction, watershed transform.**

I. INTRODUCTION

FROM the estimation of the forest resources and biomass to species identification or tree growth model construction, individual tree crown detection and delineation (ITCD) is one of the most important steps in forest resource investigation and management [8], [23], [26]. With the rapid development of remote sensing technology, the spectrum and spatial resolution have undergone a significant improvement. High-resolution aerial photos and satellite images from IKNOS, QuickBird, and others were first introduced in ITCD research [2], [4], [5], [10], [12], [24]. Various tree detection and crown delineation algorithms were developed to process passive imagery data collected by different sensors with cell sizes of a few centimeters to a few meters [11]. Active sensors such as LiDAR were later introduced, and LiDAR (first airborne then terrestrial) data are becoming mainstream in ITCD studies because they reveal the three-dimensional (3-D) structure of trees [28].

ITCD algorithms usually involve a two-step procedure: individual tree detection and tree crown delineation. A wide variety of methods have been introduced to address different types of imagery in a range of forest conditions [2], [5], [15], [19], [23].

Existing algorithms often use local reflectance maxima to detect tree apexes and local minima to delineate the crown boundaries [24]. Some representative individual tree-detection methods are local maximum filtering, image binarization, multiscale analysis, and template matching. Tree-delineation methods can be broadly grouped into three categories: valley following, region growing, and watershed segmentation. A more detailed description of these algorithms can be found in [11].

Until recently, ITCD is mostly performed on either imagery (multispectral or hyper-spectral) or LiDAR [28] collected by manned aircrafts or satellites. However, these data can be expensive to acquire or may not satisfy the specific requirements on timing and spatial resolution. For example, commercial satellite images with a resolution of 50 cm may not be able to detect trees with smaller sizes. Unmanned aerial vehicles (UAVs) are an advanced sensor-carrying platform that can be deployed quickly, frequently, and cost-effectively; high-resolution data products (mainly orthophoto, 3-D point cloud, and digital surface model) that cover an area from a few hundred square meters to a few km^2 can easily be generated. The data acquired from UAVs

bridge the gap of *in situ* ground survey and large-scale airborne or space-borne remote sensing.

UAV-acquired images and the derived products had been used for forest inventory and tree detection studies. A plot-based approach was proposed by Recio *et al.* [20] to detect fruit trees from high-spatial-resolution (0.5 m) aerial images. Based on the generated photogrammetric point cloud, Kattenborn *et al.* [9] applied a pouring algorithm for single tree detection and achieved 86.1% mapping accuracy. Malek *et al.* [16] applied an extreme learning machine classifier to detect palm trees in UAV images. Lin *et al.* [14] used UAV oblique images to detect individual trees in residential environments. Birdal *et al.* [1] estimated the tree heights in a coniferous urban forest with UAV images of 6.41 cm resolution. A correlation of 94% and a root-mean-square error of 28 cm were achieved. Panagiotidis *et al.* [18] used UAV-sensed high-resolution imagery through photogrammetry and structure from motion to estimate the tree heights and crown diameters.

For an image with cell spacing down to a few centimeters, many details of the tree canopy can be presented. Normally, it can be expected that with the improved resolution in UAV imagery, accurate, and detailed information of an individual tree and its crown boundary can be better defined. However, for automated ITCD algorithms, too many details can become a source of problem. As the spatial resolution increases, branches, twigs, and leaves with varying illumination and shadow can be discernible in the image, which causes a large within-crown spectral variation. This issue is also true for nontree background objects (bare ground or shrub and grass growing on the ground). This enhanced within-class brightness heterogeneity can affect all general image classification or segmentation algorithms [26]. Directly applying conventional image segmentation algorithms such as watershed algorithm on UAV images often results in severe over-segmentation, consequently leading to large commission error.

To mitigate this problem, some multiscale analysis and image-smoothing methods were developed (as reviewed in [11]). A transect approach [19] was proposed to detect 6-year-old coniferous trees and delineated individual crowns from color infrared (CIR) aerial photos with a spatial resolution of 5 cm. This method treated local brightness (obtained from an absolute difference image of the near-infrared and red spectral bands) maximum points as potential tree centers and introduced several transects, which extended outward from a tree apex; the crown boundary was determined at the point with the maximum rate of change in the transect. Erikson [3] presented a region growing method to segment individual tree crowns in CIR aerial photos with a pixel size of 10 cm. These two early studies worked on CIR photos and achieved tree detection rates of more than 90%.

The watershed segmentation approach is widely used to segment imagery for tree crown delineation [8]. It has the advantages of high efficiency and edge delineation accuracy. The marker-controlled watershed segmentation performs better if the foreground objects and background locations are also marked and used as the input. However, the watershed segmentation algorithm is sensitive to noise and the large spectral variation in the image, which can cause an over-segmentation of the input image. Thus, a preprocessing step to generate a smooth and clean input image is often required. Furthermore, in the pretreatment process, it is desirable to preserve the edge information and achieve minimum heterogeneity in the individual-tree-crown level.

A Gaussian smoothing filter and morphological filter were tested in our preprocessing to reduce the crown heterogeneity and background interference in UAV images; however, the final segmentation result was unsatisfactory. Consequently, other image preprocessing method is required to reduce the within-class spectral variation while maintaining the object edge.

In this paper, we propose the bias field estimation, which is a technique originally developed to correct for the bias value in magnetic resonance (MR) images as an effective method to reduce the within-canopy spectral variation for UAV high-resolution images. Although this technique is commonly used in medical image processing, we did not find its application in the remote sensing field.

From the estimated bias field, a bias corrected image can be obtained. We initially ran the segmentation test on the corrected images. However, because the spectral variation in UAV images is so strong, the over-segmentation cannot be effectively resolved even after the bias field correction. Instead, we found that the bias correction model (bias field) is more suitable for image processing with its smoothed reflectance changes.

We demonstrated the effectiveness of this approach by comparing the tree detection and crown delineation results to those derived from other methods. The ground truth was obtained using visual interpretation; the outline of each individual tree crown was manually drawn to create a stem polygon layer. The segmentation results were compared to the reference; using F-score index as the main indicator, we evaluated the accuracy of different methods in extracting the crown canopy in the UAV images. We also tested this method on some closed-canopy sites to determine whether it is applicable to other forest conditions.

The remainder of this paper is organized as follows. Section II briefly introduces the data collection process; Section III describes our proposed method; Section IV presents the segmentation results and accuracy assessment; Section V discusses some parameter considerations and method applicability extension; and Section VI concludes our paper.

II. DATA COLLECTION

The raw photos were collected with a multirotor UAV (Phantom 3 Advanced, DJI, Shenzhen, China) on March 2, 2017, in a forest nursery (see Fig. 1) in Fujian Province, China. The onboard RGB camera has a CMOS sensor with 12.4 M effective pixels; the field of view is 94° with an f/2.8 lens.

The flight height was 60 m above ground, and the longitudinal overlap and side overlap were set to be 90% and 60%, respectively. After setting the mission parameters (mission area, flying height, overlap, etc.), the waypoints were transmitted to the drone, which automatically executed the task. In total, 135 geotagged photos were acquired in approximately 10 min. Using the Pix4Dmapper (Pix4D SA, Lausanne, Switzerland) software, an ortho-image was produced by mosaicing those photos together

This article has been accepted for inclusion in a future issue of this journal. Content is final as presented, with the exception of pagination.

HUANG *et al.*: INDIVIDUAL TREE CROWN DETECTION AND DELINEATION FROM VERY-HIGH-RESOLUTION UAV IMAGES BASED ON BIAS   3
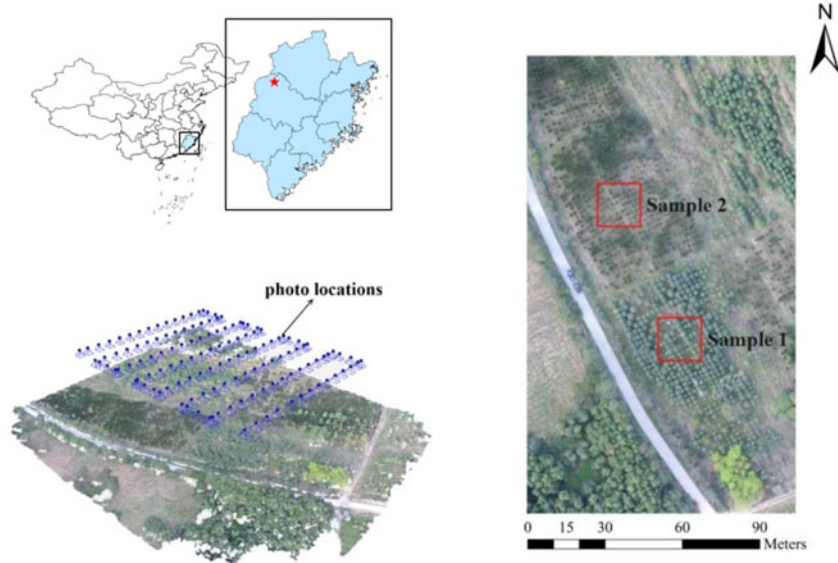
Fig. 1. Data acquisition from the study area. Upper left: the red star shows the location of the study area; Lower left: an oblique perspective image of the dense point cloud created from pix4Dmapper: the blue dots and rectangles above the point cloud represent the locations of the photos collected by the UAV when it flew above the study area; Right: an ortho-image of the study area and the locations (red rectangles) of Samples 1 and 2.

and correcting for the topographic and camera distortions. The ortho-image covers an area of approximately 0.366 km^2 with the spatial resolution of 2.54 cm.

Then, the UAV high-resolution ortho-image was used as the data source in this study. ENVI was used to clip two sample plots (both plots were located on a flat terrain and were 25 m × 25 m in size) from the image. The trees in Sample 1 are broad-leaved *Osmanthus fragrans*; their crown diameters are 0.9–3.3 m, and the tree height is between 2.05 and 4.16 m. The crown shape is hemisphere-like; most trees are in good living conditions. The trees in Sample 2 are coniferous *Podocarpus macrophyllus* with a cone-shaped crown; the tree height ranges from 1.5–3.56 m, and the crown diameters are from 0.4 to 1.8 m.

III. METHODOLOGY

Our proposed procedure can be divided into three steps: data preprocessing, image segmentation, and accuracy evaluation at the individual tree scale (see Fig. 2).

During data preprocessing, we used local intensity clustering (LIC) [13] to estimate the bias field of the UAV image; then, the output results were linearly normalized and brightness-stretched to generate the bias field images.

In the segmentation stage, the marker-controlled watershed algorithm was applied to the bias field image.

Finally, the segmentation results are evaluated by comparing them to the manually drawn individual tree crown polygons, which could be considered the ground truth. The F-score is the main accuracy evaluation index.

All segmentation tests presented here were conducted in MATLAB.

A. Bias Field Image

With the improved spatial resolution, tree crowns in the UAV image contain more details. The spectral heterogeneity also
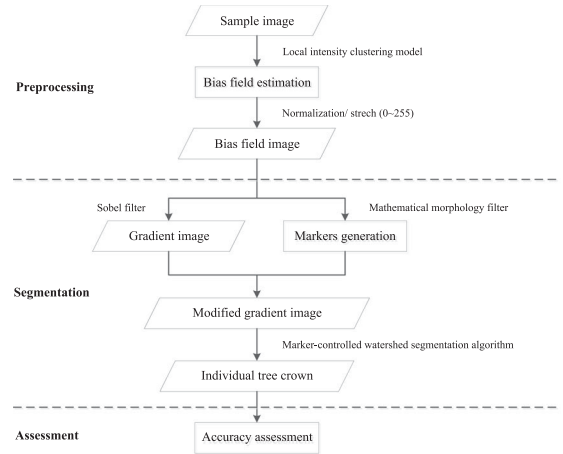

Fig. 2. Flowchart of the proposed tree crown segmentation approach.

increases, which makes the UAV image-based segmentation results difficult to achieve the individual tree identification goal. Directly removing the image spectral heterogeneity in the crown (e.g., by down-sampling, Gaussian filter, and mathematical morphology filter) is not always sufficient to meet the input image requirements of ITCD.

LIC method built a local gray density model for the observed image. Assuming that the observed image is I, the true (bias-corrected) image is J, the bias field is b, and n is the zero-mean Gaussian noise, the image model can be written in the form of

$$I = b \cdot J + n \qquad (1)$$

with the following assumptions:
1) The bias field b is assumed to be smoothly varying.
2) The true image J measures an intrinsic physical property of the objects being imaged, which is assumed to be piecewise (approximately) constant.

Bias field $b(y)$ characterizes the local intensity clustering feature. The model building process is in fact a trial to detect the intrinsic structure of the image. In other words, the observed image can be divided into a bias field and a piecewise constant image.

From assumption 1, in each sub region o_y whose subregional cluster center is y, there is

$$b(y) \approx b(x) \tag{2}$$

where $b(x)$ is the bias field in the unit pixel, whose center is x. From assumption 2, J can be represented by a group of constant c_i. Let $b(y)c_i$ express the observed image as a combination of subregions where $b(y)$ and c_i describe the observed image in the local and global scales, respectively.

Based on the fitting error between I and $b(y)c_i$, the LIC model follows

$$F_y = \sum_{i=1}^{N} \int_{o_y} K(\alpha)|I(x) - b(y)c_i|^2 dx \tag{3}$$

as an intensity clustering standard in each neighborhood o_y. $K(\alpha)$ is introduced as a nonnegative window function, which is also called a kernel function, such that $K(\alpha) = 0$ for $x \notin o_y$. Considering the intensity distribution, the kernel function is selected as a truncated Gaussian function defined by

$$K(\alpha) = \begin{cases} \frac{1}{a} e^{\frac{-|\alpha|^2}{2\sigma^2}}, for \ |\alpha| \leq \rho \\ 0, otherwise \end{cases} \tag{4}$$

where α is a normalization constant such that $\int K(\alpha) = 1$; σ is the standard deviation (or the scale parameter) of the Gaussian function, and ρ is the radius of the neighborhood o_y. Radius ρ of the neighborhood o_y should be appropriately selected according to the degree of intensity inhomogeneity. For UAV images of tree crowns with more localized intensity inhomogeneity, the bias field b varies more rapidly; therefore, the approximation in (2) is valid only in a smaller neighborhood, so ρ should be set at a small numerical value.

According to (3), if we want to obtain a good fitting result, we can build an energy equation by defining

$$\varepsilon = \int F_y dy \tag{5}$$

and minimizing ε for all y in Ω(refer to the image domains).

In order to estimate the bias field, the level set function ϕ is introduced to simplify the contour curve evolution process. Ω_i is the region identified as a target, $M_1(\phi)(M_1(\phi) = H(\phi))$ is its membership function, and $M_2(\phi)(M_2(\phi) = 1 - H(\phi))$ is the membership function of the background, where H is the *Heaviside* function. Equation (5) can be rewritten as

$$\varepsilon = \int \sum_{i=1}^{N} \int_{\Omega} e_i(x) M_i(\phi(x)) dx \tag{6}$$

where $e_i(x) = I^2 1_K - 2c_i I(b^*K) + c_i^2 (b^2 * K)$, "*" is the convolution operation, and $1_K(x) = \int K(\alpha) dy = 1$.

Thus, the energy function ε is related to the level set function ϕ, constant c and bias field b. By keeping one variable fixed
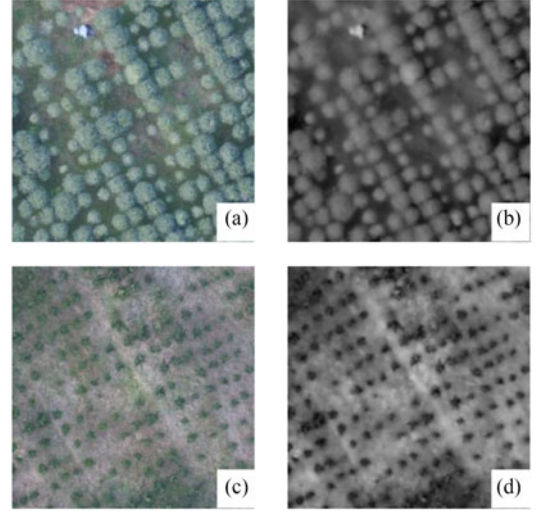

Fig. 3. Original RGB images of (a) Sample 1 and (c) Sample 2, and (b) and (d) are their corresponding bias field images.

and updating the other two by iterative computation, we can simultaneously segment the image and estimate the bias field.

Because this method was designed for image segmentation in the presence of intensity inhomogeneities, we directly applied this method to the UAV images in early experiments, but it failed to correctly segment the individual tree crown. The intensity inhomogeneity was simply too much to handle.

However, the slow-varying property of the estimated bias field can be effectively used for further image processing. We applied the linear normalization function to the original bias field b that was derived from the LIC method

$$\hat{b} = \frac{b - b_{\min}}{b_{\max} - b_{\min}} * 255 \tag{7}$$

where $b_{\max}$ and $b_{\min}$ are the maximum and minimum values in b, respectively. $\hat{b}$ can be converted into a gray-scale image for visualization and processing (see Fig. 3).

Comparing the two right column images in Fig. 3, we found that for both coniferous and broadleaf trees, the spectral heterogeneity in individual tree crowns is suppressed to a great extent in the bias field images, whereas most canopy boundary features are relatively well maintained.

Normally, in medical image processing, the segmentation is performed on the bias-corrected image; however, we found that even after the bias correction, the intensity inhomogeneities in the bias-corrected image remained high and challenging for the watershed segmentation algorithm. Thus, we instead applied the watershed segmentation algorithm to the bias field image. We did not find any segmentation study on the bias field image, so we believe that this study is the first of its kind.

In the following analysis, we used the bias field image as an input to the marker-controlled watershed algorithm. To compare with other image processing alternatives and evaluate the results, the segmentation outputs will be overlaid on the original image layer.
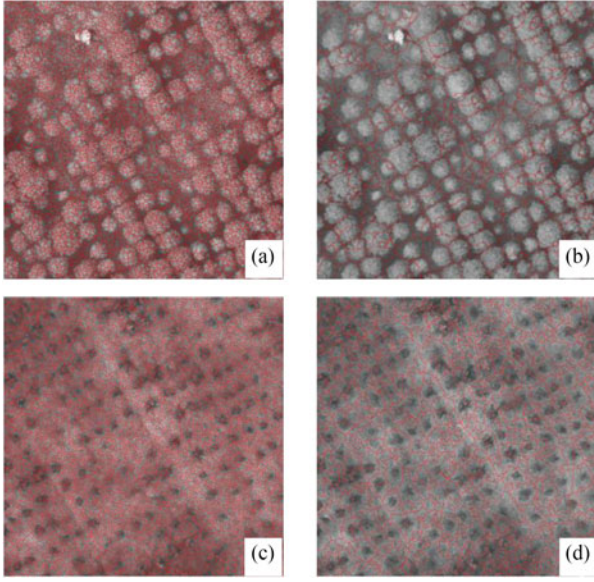
Fig. 4. Contrast of the direct watershed segmentation results based on (a) and (c) the original images and (b) and (d) bias field images of Samples 1 and 2.

B. Mathematical Morphology Filter

The intensity should smoothly vary in the bias field image now, but it requires further processing to reduce the effect of the intensity variation. First, a Sobel edge mask was applied to compute the gradient magnitude as the segmentation function; next, we used morphological techniques (reconstruction-based opening and closing operation, [21]) to remove the noise and fine texture in the tree crowns. The reconstruction-based opening and closing operation can further smooth the fine texture in individual tree crowns and generate no boundary offset. This filter was applied to the bias field image. Based on the average tree crown diameters, filters with window sizes of 9×9 and 5×5 were selected for Samples 1 and 2, respectively.

C. Marker-Controlled Watershed Segmentation Algorithm

The watershed segmentation algorithm (or watershed transform) is a type of region-growing algorithm in essence, but it sets the growing seeds at the local minima. The watershed transform finds "catchment basins" and "watershed ridge lines" in an image by treating it as a surface, where light pixels are peaks and dark pixels are valleys. Because of the high spatial resolution of UAV images, there may be more than one intensity maximum in each tree crown. Directly applying the watershed algorithm can cause severe over-segmentation [see Fig. 4(a) and (c)]. Marking the local extremes is an effective solution to this problem. Generally, there are internal and external markers. To extract the individual tree crowns, tree tops are labeled as the internal markers by applying a local maximum filter, and background pixels are labeled as the external markers. The readers are referred to Wang *et al.* [24] and Jing *et al.* [8] for more information about the marker-controlled watershed transform.

In general, the watershed transform follows these steps: using a grayscale image as the input, a fixed window size local maximum filter was used to detect the treetops and generate markers.

The window size of the local maximum filter depends on the average size of the tree crown in the sample plots (as measured in the field and estimated from the ortho-image). Then, the image was modified by the minima-imposing operation to ensure that it only has minima at the predefined internal marker locations. Finally, the watershed-based segmentation was executed on the modified gradient magnitude image to produce the final result.

IV. RESULTS

We compared and evaluated the segmentation results of different processing options for Samples 1 and 2.

First, we demonstrated that the bias field image provided a better-quality starting point for image segmentation. As shown in Fig. 4, with no other preprocessing (morphological filtering and marker generating), the segmentation results (red polygons superimposed on the gray image) of the direct watershed algorithm based on the bias field images of Samples 1 and 2 are better than those based on the original images. Although many errors remain, over-segmentation is significantly reduced in the bias field images.

Fig. 5 shows the marker-controlled watershed segmentation results using both original images [Fig. 5(a), (b), (e), and (f)] and bias field images [Fig. 5(c), (d), (g), and (h)] of Samples 1 and 2. Similar to the bias field image processing steps, a Sobel edge mask and a reconstruction-based opening and closing operation were applied to the original image before the final watershed segmentation. The conventional marker-controlled watershed algorithm that marked both foreground and background does not perform well, as shown in Fig. 5(a), (e), (c), and (g). Fig. 5(b), (f), (d), and (h) displays the results using only the internal (foreground object) markers, and higher accuracy was achieved in Fig. 5(d) and (h), which is based on the bias field images.

A closer look at the segmentation results clearly shows the differences. Fig. 5(a), (b), (e), and (f) shows the output of the marker-controlled watershed algorithm applied to the original images with different marker settings. For Sample 1, some crowns were not detected, and some overlapping crowns were incorrectly identified as one object; for Sample 2, the over-segmentation error is obvious. They indicated clearly the Sobel operator and morphological filter were not effective in generating desirable images for watershed transform. Fig. 5(c), (d), (g), and (h) shows the results of the marker-controlled watershed algorithm applied to the corresponding bias field images. For both Samples 1 and 2, almost all trees were correctly detected. In particular, for Sample 2, good accuracy was obtained: most segmented crown contours closely or tightly followed the boundary of the crown; although for Sample 1, some contours failed to completely match the reference crown boundary, and the overlapping rate was more than 50%.

We also compared the effects of internal and external markers on the segmentation results. If both internal and external markers were applied, the results are less ideal than those using only the internal markers. The best results are from bias field images using only the internal markers as shown in Fig. 5(d) and (h), where the crown contours are closer to the real crown border, and

This article has been accepted for inclusion in a future issue of this journal. Content is final as presented, with the exception of pagination.

6   IEEE JOURNAL OF SELECTED TOPICS IN APPLIED EARTH OBSERVATIONS AND REMOTE SENSING
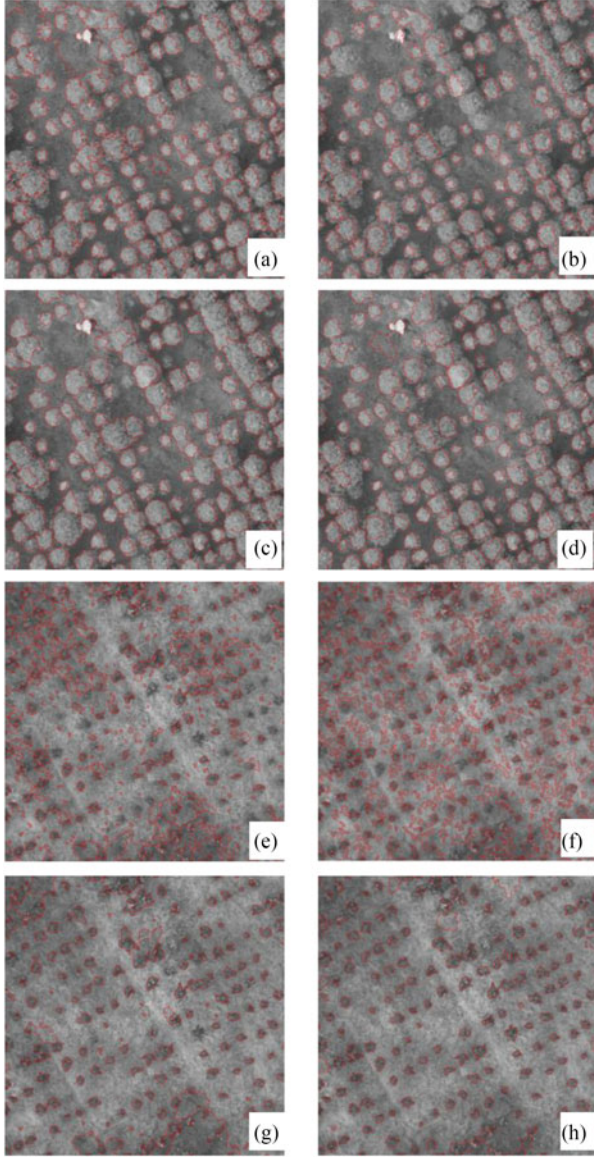

Fig. 5.   Marker-controlled watershed segmentation results based on the original image of Samples 1 and 2 using both internal and external markers (a) and (e) and only the internal markers (b) and (f); The marker-controlled watershed segmentation results based on the bias field image of Samples 1 and 2 using both internal and external markers (c) and (g) and only internal markers (d) and (h).

individual trees are not mistakenly merged or interconnected. The difference in performance may be caused by the background interference; the presence of the background (noncrown objects including understory vegetation and bare soil) is substantial in our study site. To compare the results obtained by different algorithms and settings, we conducted a quantitative accuracy evaluation as follows.

Accuracy assessment is a key step in segmentation-based image-processing techniques [25]. It is beneficial to improve the efficiency of the existing algorithms and is of guiding significance to the development of new segmentation techniques. The ITCD accuracy index can be evaluated from individual trees to the plot scale, and two aspects are examined [28]

1) Point accuracy: Tree detection accuracy.
2) Polygon accuracy: Segmentation quality of the crown contour.

The more comprehensive verification method is at the individual tree scale. The accuracy rate, recall rate, and F-score are used: recall is a measure of the tree detection rate, precision is a measure of the correctness of detected trees, and the F-score indicates the overall accuracy considering the omission and commission errors [6].

The red polygons in Fig. 6 represent the hand-drawn crown boundaries in ArcGIS (used as the reference for the evaluation), whereas the yellow contours are the results from the bias field image and internal-marker-controlled watershed segmentation algorithm. To perform the accuracy assessment, we compared the algorithm segmentation results with the reference crowns. The trees at the edge of the sample plot with incomplete crown shapes were not included in the accuracy assessment process.

In general, we have the following definitions:

$$\text{Accuracy rate}: A_d = \frac{N_c}{N_d} \times 100\% \qquad (8)$$

$$\text{Recall rate}: A_r = \frac{N_c}{N_r} \times 100\% \qquad (9)$$

$$\text{F} - \text{score}: F = \frac{2A_r A_d}{A_r + A_d} \qquad (10)$$

where N_c is the number of correctly segmented crowns; N_r is the number of crowns in the reference (truth value); and N_d is the total number of crowns that the algorithm can detect. Based on the spatial relationship between the segmentation results and the reference crowns, the segmentation result (N_d) can be divided into five classes: Matched, Nearly matched, Missed, Merged, and Spilt [4], [8]. Nc is counted as the sum of matched and nearly matched.

We quantitatively evaluated the segmentation accuracy in Fig. 5. For the convenience of discussion, the original image is denoted as O, and the bias field image is denoted as B; the watershed segmentation method using both internal and external markers is abbreviated as IEW; and the watershed segmentation method using only internal markers is IW. In this case, OIEW indicates that the marker-controlled watershed algorithm is applied to the original image using both internal and external markers; BIW indicates that the watershed segmentation algorithm is applied to the bias field image using only internal markers. The results in Table I show that the overall better segmentation results were achieved from the bias field images than those from the original images, particularly for Sample 2. For both samples, BIW has the best performance in terms of accuracy, recall and F-score.

V. DISCUSSION

Nowadays, readily available higher-resolution UAV images (e.g., with GSD less than 10 cm) facilitate the correct detection of small-sized trees and accurate delineation of their crown boundaries, which are difficult to achieve in traditional coarse-resolution images. The spectral heterogeneity generally

This article has been accepted for inclusion in a future issue of this journal. Content is final as presented, with the exception of pagination.

HUANG *et al.*: INDIVIDUAL TREE CROWN DETECTION AND DELINEATION FROM VERY-HIGH-RESOLUTION UAV IMAGES BASED ON BIAS
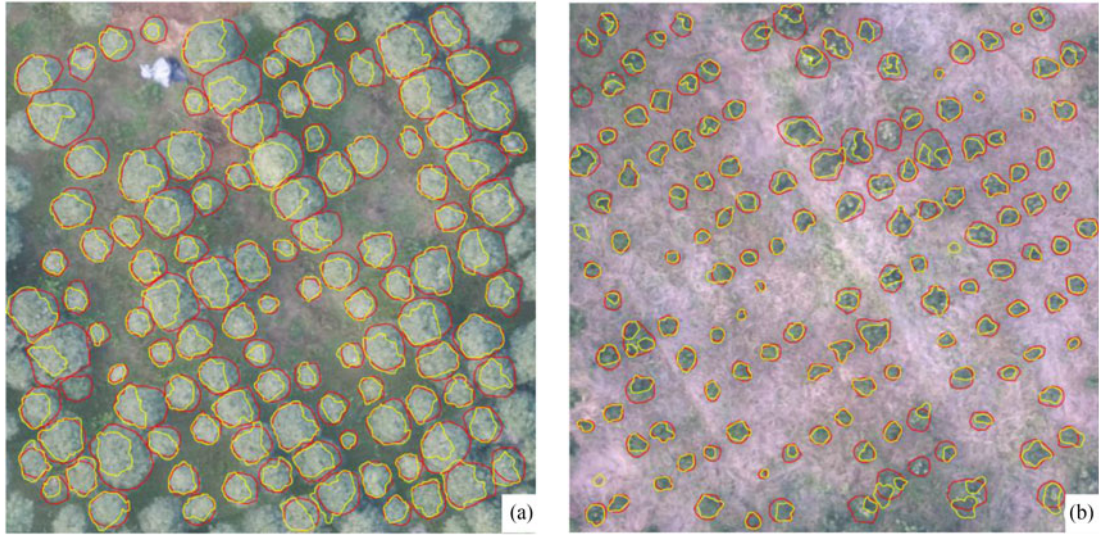
7

Fig. 6. Internal marker-controlled watershed-algorithm-generated crown segments (yellow) and the reference crowns (red), which are superimposed on the RGB images of (a) Sample 1 and (b) Sample 2.

TABLE I
NUMBER OF TREES DETECTED BY VARIOUS ALGORITHM SETTINGS AND IMAGE SOURCES AND THE CORRESPONDING INDICES

Sample	Algorithm	Nr	Nd	Nc	Accuracy	Recall	*F-score*
Sample 1	OIEW		133	72	54.1%	63.2%	58.3%
	OIW		125	86	68.8%	75.4%	72.0%
	BIEW	114	107	74	69.2%	64.9%	67.0%
	BIW		112	111	99.1%	97.4%	98.2%
Sample 2	OIEW		167	36	21.6%	26.5%	23.8%
	OIW	136	641	47	7.3%	34.6%	12.1%
	BIEW		128	104	81.3%	76.5%	78.8%
	BIW		141	129	91.5%	94.9%	93.1%

increases with the spatial resolution of images. A finer resolution implies that more computation resources and extra image processing steps are required to address the issue of within-class spectral variation. Multiscale image analysis and optical smoothing techniques were proposed to reduce the effect of brightness heterogeneity [11]. We conducted experiments using similar image smoothing (Gaussian and morphological) filters. However, these tools are not sufficiently effective to mitigate the intensity variation in the UAV images. Pouliot *et al.* [19] discussed the effect of the pixel size on the delineation accuracy of regenerating coniferous forest plantation. For their application, they found the best crown detection and delineation result at the crown-diameter-to-pixel ratio of 15 (for example, with a pixel size of 10 cm, this ratio corresponds to a crown diameter of 150 cm). A low crown-diameter-to-pixel ratio made the crown boundaries indistinctive, whereas a high ratio (equal to or greater than 19) increased the commission error because of the high within-crown brightness variation. For our study, the crown-diameter-to-pixel ratio is greater than 30 even for smaller coniferous trees; the amount of spectral variation is more prominent, which may explain why the traditional Gaussian and morphological smoothing tools and the LIC method do not work.

In the previous section, we demonstrated the advantages of the bias field image. We found that the bias field image with reduced within-crown reflectance variation was suitable for further watershed segmentation processing. We focused on the bias field image, which can be considered a description of the local intensity clustering information and not on the bias-corrected image, which retains the high within-crown spectral heterogeneity. The tree crowns in the bias field image [Fig. 3(b) and (d)] show a brightness distinction of crowns from their background, whereas the brightness smoothly varies for each crown. Thus, the corresponding tree crowns can be easily detected from the bias field images when combining with the internal marker-controlled watershed algorithm. A significant improvement (at least 20% in *F*-score) in crown detection can be obtained from the bias field image processing compared to those from the original image.

Samples 1 and 2 show opposite image properties. In Sample 1, the tree crowns have higher reflectance, and the background is dark; in Sample 2, the crowns are dark, and the background is brighter. This issue can pose challenges to the processing algorithms. However, with the bias field image, the crown detection rates and delineation results from both sites are impressive; and this demonstrates the robustness of our proposed technique.

This article has been accepted for inclusion in a future issue of this journal. Content is final as presented, with the exception of pagination.

8

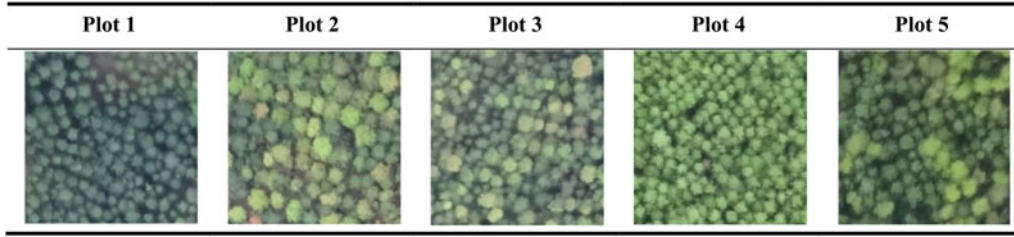IEEE JOURNAL OF SELECTED TOPICS IN APPLIED EARTH OBSERVATIONS AND REMOTE SENSING

Fig. 7. UAV images of forest plots with higher tree densities.
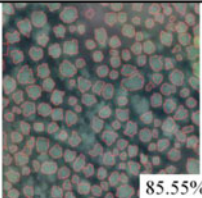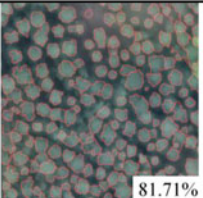
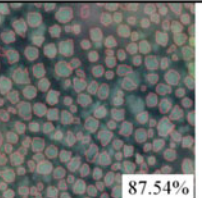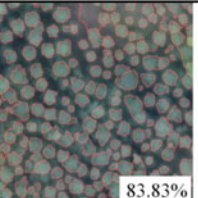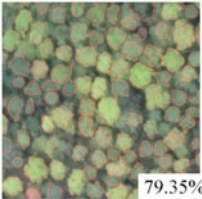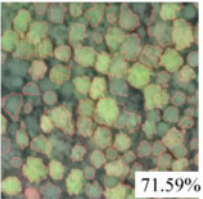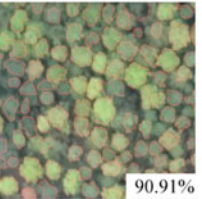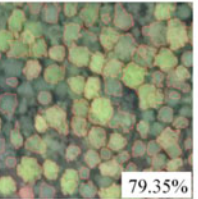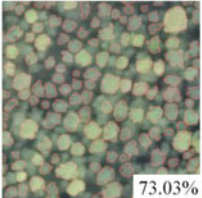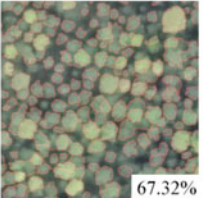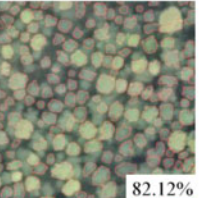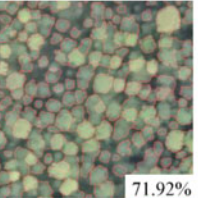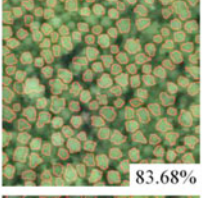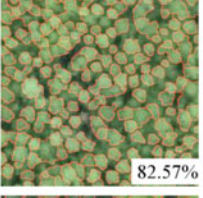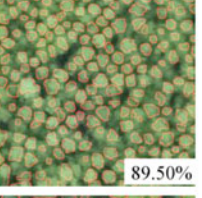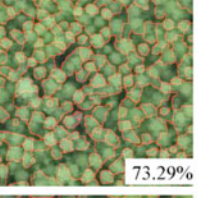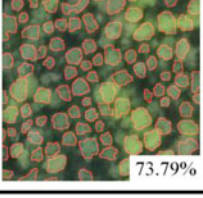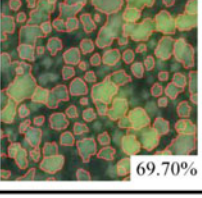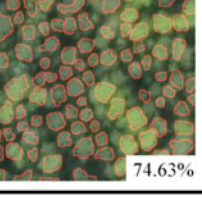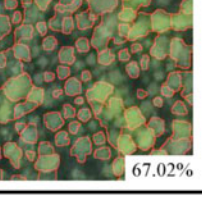Fig. 8. Comparison of the segmentation results based on different input images [original images (O) and bias field images (B)] and different segmentation methods [watershed with both external and internal markers (IEW) and watershed with only internal markers (IW)]. The *F*-score is also displayed on the lower right corner for each combination.

We further tested this technique to some UAV-derived images of forested areas with higher canopy cover. Fig. 7 shows five different forest plots with sizes of 25 m × 25 m. Plots 1–3 were extracted from an ortho-image with a GSD of 6.48 cm, whereas Plots 4 and 5 have GSDs of 10.86 cm and 11.83 cm, respectively. These plots show some dense forests with both coniferous and broadleaved trees of various sizes. Similarly, the marker-controlled watershed algorithm was applied to the original images and their bias field counterparts. The ITCD results are shown in Fig. 8 with the computed *F*-scores. Fig. 8 shows that the marker-controlled watershed algorithm performed similarly well for both original images and bias field images. However, the BIW (using only the internal markers on the bias field image) always achieved the highest *F*-score, although it was only

few percentages higher in some cases. This result again proves the validity of our proposed method because it can be applied to denser forest areas.

Unlike Samples 1 and 2, where both trees (objects) and background (nontree objects) have fairly similar spatial coverage, Plots 1–5 show mostly compact tree crowns, and the nontree background is almost invisible or negligible. Different image compositions with the reduced spatial resolution can affect the segmentation results.

For the segmentation process, the marker-controlled watershed algorithm normally uses both internal and external markers. Considering the apparent background presence in Samples 1 and 2, we removed the external markers in the algorithm and obtained better accuracy using only the internal markers. The complicated background objects may confuse the algorithm and cause omission errors.

We will continue to perform the follow-up research works such as the quantitative estimation of image heterogeneity and individual tree detection based on an image-matching point cloud, and we will collect more field samples to improve the validity and applicability of this method. More studies are required to better integrate the associated hierarchical segmentation maps of imagery to produce accurate and complete tree crown maps for forest inventory purposes.

VI. Conclusion

Compared with the aerial photos and satellite images, UAV-based imaging is quick, efficient, and cost-effective. More up-to-date and accurate forest inventory information can be retrieved from the UAV-derived very high-resolution images. However, the high resolution can be a "double-edged sword" because too much details and high spectral heterogeneity in the images can cause some traditional image processing algorithms to fail in the application of object classification and segmentation.

In this paper, we proposed a new approach that uses the bias field image as a substitute for the original RGB image in ITCD research and uses the smooth varying feature in the bias field. In medical image processing, the bias field image is a byproduct to obtain the corrected image and was rarely used in other applications. Our study found that the bias field image had some desirable properties: the canopy boundaries are effectively maintained while the intensity inhomogeneities within the crown are largely suppressed. And the method based on the bias field and marker-controlled watershed algorithm is well suited for extracting individual tree crowns from UAV-derived very high-resolution images with marked spectral heterogeneity. Combining with the marker-controlled watershed algorithm, the method can achieve notably good results with F-scores above 90%.
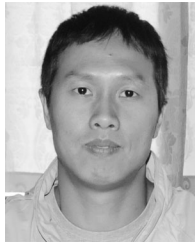
References

[1] A. C. Birdal, U. Avdan, and T. Türk, "Estimating tree heights with images from an unmanned aerial vehicle," *Geomatics Natural Hazards Risk*. vol. 8, no. 2, pp. 1144–1156, 2017.

[2] T. Brandtberg, "Automated delineation of individual tree crowns in high spatial resolution aerial images by multiple-scale analysis," *Mach. Vision Appl.*, vol. 11, pp. 64–73, 1998.

[3] M. Erikson, "Segmentation of individual tree crowns in colour aerial photographs using region growing supported by fuzzy rules," *Can. J. Forest Res.*, vol. 33, no. 8, pp. 1557–1563, 2003.

[4] F. A. Gougeon, "A crown-following approach to the automatic delineation of individual tree crowns in high spatial resolution aerial images," *Can. J. Remote Sens.*, vol. 21, no. 3, pp. 274–284, 1995.

[5] F. A. Gougeon and D. G. Leckie, "The individual tree crown approach applied to IKONOS images of a coniferous plantation area," *Photogrammetric Eng. Remote Sens.*, vol. 72, pp. 1287–1297, 2006.

[6] H. Hamraz, M. A. Contreras, and J. Zhang, "A robust approach for tree segmentation in deciduous forests using small-footprint airborne LiDAR data," *Int. J. Appl. Earth Observ. Geoinf.*, vol. 52, pp. 532–541, 2016.

[7] C. Hung, M. Bryson, and S. Sukkarieh, "Multi-class predictive template for tree crown detection," *ISPRS J. Photogrammetry Remote Sens.*, vol. 68, no. 3, pp. 170–183, 2012.

[8] L. Jing, B. Hu, J. Li, and T. Noland, "An individual tree crown delineation method based on multi-scale segmentation of imagery," *ISPRS J. Photogrammetry Remote Sens.*, vol. 70, no. 3, pp. 88–98, 2012.

[9] T. Kattenborn, M. Sperlich, K. Bataua, and B. Koch, "Automatic single tree detection in plantations using UAV-based photogrammetric point clouds," *Int. Arch. Photogramm. Remote Sens. Spat. Inf. Sci.* vol. XL-3, pp. 139–144, 2014.

[10] Y. Ke and L. J. Quackenbush, "Forest species classification and tree crown delineation using QuickBird imagery," in *Proc. ASPRS Annu. Conf.*, Tampa, FL, USA (Bethesda, MD, USA: American Society for Photogrammetry and Remote Sensing), May 2007.

[11] Y. Ke and L. J. Quackenbush, "A review of methods for automatic individual tree-crown detection and delineation from passive remote sensing," *Int. J. Remote Sens.*, vol. 32, no. 17, pp. 4725–4747, 2011.

[12] M. Larsen, "Crown modelling to find tree top positions in aerial photographs," in *Proc. 3rd Int. Airborne Remote Sens. Conf. Exhib.*, Copenhagen, Denmark (Ann Arbor, MI, USA: ERIM International), Jul. 1997, pp. 428–435.

[13] C. Li, R. Huang, Z. Ding, J. C. Gatenby, D. N. Metaxas, and J. C. Gore, "A level set method for image segmentation in the presence of intensity inhomogeneities with application to MRI," *IEEE Trans. Image Process.*, vol. 20, no. 7, pp. 2007–2016, Jul. 2011.

[14] Y. Lin, M. Jiang, Y. Yao, L. Zhang, and J. Lin, "Use of UAV oblique imaging for the detection of individual trees in residential environments," *Urban Forestry Urban Greening*, vol. 14, no. 2, pp. 404–412, 2015.

[15] T. Liu, J. Im, and L. J. Quackenbush, "A novel transferable individual tree crown delineation model based on Fishing Net Dragging and boundary classification," *ISPRS J. Photogrammetry Remote Sens.*, vol. 110, pp. 34–47, 2015.

[16] S. Bazi Malek, Y. Alajlan, N. AlHichri H., and F. Melgani, "Efficient framework for palm tree detection in UAV Images," *IEEE J. Sel. Topics Appl. Earth Observ. Remote Sens.*, vol. 7, no. 12, pp. 4692–4703, Dec. 2014.

[17] B. Mora, M. A. Wulder, and J. C. White, "Segment-constrained regression tree estimation of forest stand height from very high spatial resolution panchromatic imagery over a boreal environment," *Remote Sens. Environ.*, vol. 114, no. 11, pp. 2474–2484, 2010.

[18] P. Panagiotidis, A. Abdollahnejad, P. Surový, and V. Chiteculo, "Determining tree height and crown diameter from high-resolution UAV imagery," *Int. J. Remote Sens.*, vol. 38 pp. 2392–2410, 2017.

[19] D. A. Pouliot, D. J. King, F. W. Bell, and D. G. Pitt., "Automated tree crown detection and delineation in high-resolution digital camera imagery of coniferous forest regeneration," *Remote Sens. Environ.*, vol. 82, pp. 322–334, 2002.

[20] J. A. Recio, T. Hermosilla, L. A. Ruiz, and J. Palomar, "Automated extraction of tree and plot-based parameters in citrus orchards from aerial images," *Compute. Electron. Agriculture*, vol. 90, no. 2, pp. 24–34, 2013.

[21] P. Soille, *Morphological Image Analysis: Principles and Applications*. Berlin, Germany: Springer, 1999.

[22] C. Vega, A. Hamrouni, S. E. Mokhtari, J. Morel, J. Bock, and J. P. Renaud, "PTrees: A point-based approach to forest tree extraction from lidar data," *Int. J. Appl. Earth Observ. Geoinf.*, vol. 33, no. 1, pp. 98–108, 2014.

This article has been accepted for inclusion in a future issue of this journal. Content is final as presented, with the exception of pagination.

10   IEEE JOURNAL OF SELECTED TOPICS IN APPLIED EARTH OBSERVATIONS AND REMOTE SENSING

[23] L. Wang, "A Multi-scale approach for delineating individual tree crowns with very high resolution imagery," *Photogrammetric Eng. Remote Sens.*, vol. 76, no. 4, pp. 371–378, 2010.

[24] L. Wang, P. Gong, and G. S. Biging, "Individual tree-crown delineation and treetop detection in high-spatial-resolution aerial imagery," *Photogrammetric Eng. Remote Sens.*, vol. 70, no. 3, pp. 351–357, 2004.

[25] B. Wu, S. Lin, and G. Zhou, "Quantitatively evaluating indexes for object-based segmentation of high spatial resolution image," *Geo-Inf. Sci.*, vol. 15, no. 4, pp. 567–573, 2013.

[26] D. Yin and L. Wang, "How to assess the accuracy of the individual tree-based forest inventory derived from remotely sensed data: a review," *Int. J. Remote Sens.*, vol. 37, no. 19, pp. 4521–4553, 2016.

[27] Z. Zhen, L. J. Quackenbush, S. V. Stehman, and L. Zhang, "Agent-based region growing for individual tree crown delineation from airborne laser scanning ALS data," *Int. J. Remote Sens.*, vol. 36, no. 7, 1965–1993, 2015.

[28] Z. Zhen, L. Quackenbush, and L. Zhang, "Trends in automatic individual tree crown detection and delineation—Evolution of LiDAR data," *Remote Sens.*, vol. 8, no. 4, p. 333, 2016.

Xu Li was born in Hebei Province, China in 1991. He received the B.S. degree in environment and urban and rural planning management from Shijiangzhuang University, Shijiazhuang, China, in 2015. He is currently working toward the M.S. degree in cartography and geographical information system at Fuzhou University, Fuzhou, China.

His research interests include UAV remote sensing of forest resources, High resolution image and image matching point cloud processing, and information extraction.

Hongyu Huang received the M.Sc. degree in electronic engineering from the University of Southern California, Los Angeles, CA, USA, in 2001.

He has been with the Key Laboratory of Spatial Data Mining and Information Sharing, Ministry of Education, Fuzhou University, Fuzhou, China, since 2003. His current research interests include laser scanning, 3-D modeling, UAV remote sensing, and information extraction from 3-D point cloud and high-resolution images.

Chongcheng Chen received the B.S. and M.S. degrees in hydrogeology and engineering geology from Chengdu College of Geology, Chengdu, China, in 1989 and 1992, respectively. He received the Ph.D. degree in cartography and GIS from the Institute of Geography and Resources, Chinese Academy of Sciences, in 2000.

Since 2006, he has been a Full Professor at Fuzhou University, China. He has more than 23 years of experience of research and education in fields of geoinformatics and computer applications. He initiated the Geographic Information System (GIS) development and application in Fuzhou University. He has been dedicating to bridge the gap between innovative IT and earth science research under the umbrella of "Digital/Smart Earth," and promotin geospatial technology to inoculate with applications in broad fields of natural resources, environment ecology, and government management. His research interests include spatial data mining, geographical knowledge cloud, spatial decision system, geo-visualization and virtual geographic environment, cultural heritage documentation, and tourism information service. He has coauthored more than 180 referred journal and conference papers, held more than 21 Chinese patents and software copyrights.